Title
Retinal Nerve Fiber Layer Reflectance for Early Glaucoma Diagnosis

Journal
Journal of Glaucoma, 23(1)

ISSN
1057-0829

Authors
Liu, Shuang
Wang, Bingqing
Yin, Biwei
et al.

Publication Date
2014

DOI
10.1097/ijg.0b013e31829ea2a7

Peer reviewed

Published in final edited form as:
J Glaucoma. 2014 January ; 23(1): . doi:10.1097/IJG.0b013e31829ea2a7.

Retinal nerve fiber layer reflectance for early glaucoma diagnosis

Shuang Liu, Ph.D.[1,2], **Bingqing Wang, B.S.**[1], **Biwei Yin, M.S.**[3], **Thomas E. Milner, Ph.D.**[1], **Mia K. Markey, Ph.D.**[1,4], **Stuart J. McKinnon, M.D.**[5], and **H. Grady Rylander III, M.D.**[1,*]

[1]Department of Biomedical Engineering, The University of Texas at Austin, Austin, TX, 78712

[3]Department of Electrical & Computer Engineering, The University of Texas at Austin, Austin, TX, 78712

[4]Department of Imaging Physics, The University of Texas MD Anderson Cancer Center, Houston, TX, 77030

[5]Departments of Ophthalmology and Neurobiology, Duke University Medical Center, Durham, NC, 27710

Abstract

Purpose—Compare performance of normalized reflectance index (NRI) and retinal nerve fiber layer thickness (RNFLT) parameters determined from OCT images for glaucoma and glaucoma suspect diagnosis.

Methods—Seventy-five eyes from seventy-one human subjects were studied: 33 controls, 24 glaucomatous, and 18 glaucoma-suspects. RNFLT and NRI maps were measured using two custom-built OCT systems and the commercial instrument RTVue. Using area under the receiver operating characteristic (ROC) curve, RNFLT and NRI measured in seven RNFL locations were analyzed to distinguish between control, glaucomatous, and glaucoma-suspect eyes.

Results—The mean NRI of the control group was significantly larger than the means of glaucomatous and glaucoma-suspect groups in most RNFL locations for all three OCT systems ($p<0.05$ for all comparisons). NRI performs significantly better than RNFLT at distinguishing between glaucoma-suspect and control eyes using RTVue OCT ($p=0.008$). The performances of NRI and RNFLT for classifying glaucoma-suspect vs. control eyes were statistically indistinguishable for PS-OCT-EIA ($p=0.101$) and PS-OCT-DEC ($p=0.227$). The performances of NRI and RNFLT for classifying glaucomatous vs. control eyes were statistically indistinguishable (PS-OCT-EIA: $p=0.379$; PS-OCT-DEC: $p=0.338$; RTVue OCT: $p=0.877$).

Conclusions—NRI is a promising measure for distinguishing between glaucoma-suspect and control eyes and may indicate disease in the pre-perimetric stage. Results of this pilot clinical study warrant a larger study to confirm the diagnostic power of NRI for diagnosing pre-perimetric glaucoma.

[*]Corresponding Author: Mailing address:, Department of Biomedical Engineering, BME 1.108A, The University of Texas at Austin, 1 University Station, C0800, Austin, Texas 78712-1062, Phone: (512) 471-1995, Fax: (512) 471-0616, Rylander@mail.utexas.edu.
[2]Currently with Department of Neurology, Yale School of Medicine, New Haven, CT, 06510

Keywords

glaucoma; optical coherence tomography; retinal nerve fiber layer

Introduction

Glaucoma is a progressive disease characterized by loss of retinal ganglion cells and their axons in the retinal nerve fiber layer (RNFL). Multiple clinical approaches are employed for glaucoma diagnosis, including morphological assessment of the optic nerve and visual field testing. Optic nerve imaging devices such as GDx VCC (Carl Zeiss Meditec, Inc, Dublin, CA), Heidelberg Retinal Tomography (HRT, Heidelberg Engineering, GmbH, Dossenheim, Germany), and Optical Coherence Tomography (OCT) (e.g., RTVue, Optovue, Inc., Fremont, CA) are widely used to assist in glaucoma diagnosis and monitoring. Early detection of glaucoma or disease progression is important because effective treatments are available to preserve visual function.

Optical Coherence Tomography (OCT) is a noninvasive imaging method that provides high-resolution quantitative morphological information about the RNFL and optic nerve. A recent study reports a sensitivity of 85% and specificity of 94% for distinguishing between glaucoma and control eyes using RNFLT measured by the Cirrus OCT instrument.[1] Wu et al. reports that statistical RNFLT parameters for evaluating the diagnostic performance of the Spectralis OCT system (Heidelberg Engineering, Heidelberg, Germany) are good for diagnosing early perimetric glaucoma (AUC=0.895) and excellent for moderately advanced glaucoma (AUC=0.952).[2] Polarization Sensitive Optical Coherence Tomography (PS-OCT) has emerged as a candidate technique for glaucoma diagnosis. PS-OCT provides both depth-resolved morphological images, RNFLT and RNFL birefringence (Δn).[3] Studies using OCT to distinguish glaucoma-suspect vs. control eyes are inconclusive. Some studies using OCT did not find significant RNFLT differences between control and ocular hypertensive or glaucoma-suspect eyes.[4, 5] Other studies using OCT reported promising results for using changes in RNFLT to detect early structural damage in glaucoma-suspect eyes.[6–8] Determining the RNFL properties that best distinguish between control and glaucoma-suspect eyes requires further study.

In a longitudinal glaucoma study involving non-human primates using OCT, a RNFL reflectance parameter, reflectivity index (RI) was introduced for distinguishing between early onset glaucomatous vs. control eyes.[9] Study results suggest that RNFL reflectance (RI) might be an earlier indicator of glaucoma onset than RNFLT, phase retardation (PR), or birefringence (Δn).[9] A recent human study suggested that a RNFL reflectance parameter can be used for glaucoma assessment.[10] We report results of a cross-sectional study on human eyes using a normalized RNFL reflectance index (NRI) which is RI * RNFLT. Performance of RNFLT and NRI, are compared for distinguishing glaucomatous vs. control eyes and glaucoma-suspect vs. control eyes.

METHODS

Subjects and study protocol

Two study groups are presented. The first group consisted of 34 eyes (13 control, 9 glaucomatous, and 12 glaucoma-suspect) from 33 human subjects enrolled at the Eye Institute of Austin (EIA). The first study group was imaged with a custom polarization-sensitive OCT system (PS-OCT-EIA) and a commercial OCT system (RTVue). The second group consisted of 41 eyes (20 control, 15 glaucomatous, and 6 glaucoma-suspect) from 38 human subjects enrolled at the Duke Eye Center (DEC). The second group was imaged with

a second custom polarization-sensitive OCT system (PS-OCT-DEC). Both studies were designed to evaluate RNFL birefringence, RNFLT, RI, and NRI for glaucoma diagnostics. We report only the RNFLT and NRI since birefringence and RI were found to be less useful for detecting glaucoma (supplement Table e4–7). Both eyes of each study participant were imaged. For each subject with the same diagnosis for both eyes (e.g., glaucomatous), the eye providing the best quality images was selected for further analysis. For data recorded with PS-OCT instruments, three imaging measurements were recorded from each eye. The image with least number of un-processable clusters (e.g., A-scans affected by eye blinking or cases when the RNFL is outside the effective imaging depth) was selected and processed. For RTVue OCT, the eye with highest scan score index (SSI) was selected. For glaucoma patients with one glaucomatous eye and one glaucoma-suspect eye, both eyes were included in the data analysis since the study does not directly compare glaucomatous vs. glaucoma-suspect eyes. Mean-age and standard deviation together with gender distribution, mean and standard deviation of visual field mean deviation (VF MD) and visual field pattern standard deviation (VF PSD) are indicated in Table 1.

Eligibility to participate in the study was based on medical and ocular history and a comprehensive eye examination including standard disc photography and results of a Humphrey-Zeiss 24-2 (Carl Zeiss Meditec, Inc, Dublin, CA) visual field test. Inclusion and exclusion criteria and definitions are given in Table 2 and Table 3. Using the definitions in Table 3, each eye was classified as normal, glaucoma, or glaucoma suspect by a glaucoma expert at either EIA or DEC. The two studies are considered separately because the expert classification and the instrumentation were different at the two study sites.

This study was approved by the Institutional Review Boards at The University of Texas at Austin and at Duke University Medical Center (NCT #01222065).

Instrumentation

Two custom built polarization-sensitive OCT instruments (PS-OCT-EIA and PS-OCT-DEC) and one commercial OCT instrument (RTVue OCT) were employed for retinal imaging (see supplemental eTable 1). The basic design of the two custom OCT systems operating at 1060nm was described previously[3]. The RTVue uses a superluminescent diode light source with a center wavelength of 840 nm.

RNFLT and NRI calculation

For PS-OCT-EIA and PS-OCT-DEC, $RNFLT(r,\theta)$ in μm was calculated by a custom LabVIEW software program (National Instruments, Austin, Texas) to automatically detect RNFL and RPE region boundaries in each B-scan.[3, 11,12] $RNFLT(r,\theta)$ of RTVue OCT is provided by RTVue software version 4.0.5.39.

The normalized RNFL reflectance index (*NRI*) is defined as the ratio of the integrated OCT RNFL intensities (I_{RNFL}) to the average OCT intensity of a thin layer centered on the retinal pigment epithelium (*RPE*). NRI is the intensity of back-reflected light summed over the RNFL normalized by the intensity of back-reflected light measured over the RPE. The RI reported in the primate study is NRI/RNFLT. Advantages of NRI over RI are: 1) the measure is unitless whereas the RI has units of inverse length; 2) NRI is somewhat less prone to error since the pixel intensities in the RNFL are simply summed whereas in computing RI, errors in RNFLT can be introduced; 3) because NRI is a measure of the composite RNFL reflectivity, this measure is sensitive to reductions in either thickness or reflectivity.

For OCT data, we define $NRI(r,\theta)$ for one cluster at radius r and azimuth angle θ as:

$$NRI(r,\theta)=\frac{I_{RNFL_c}(r,\theta)}{\overline{I}_{RPE}} \quad (1)$$

where,

$$I_{RNFL_c}(r,\theta)=\sum_{i=1}^{N_c} I_{RNFL_i} \quad (2)$$

corresponding to the summed OCT signal intensity I_{RNFL_i} in the RNFL in one cluster, where N_a is number of pixels in cluster '*c*' located at *r* and θ.

Average OCT signal intensity within a thin layer about the retinal pigment epithelium is calculated as:

$$\overline{I}_{RPE}=\frac{\sum_{b=1}^{N_b}\left(\sum_{a=1}^{N_a} I_{RPE_a}/N_{RPE}\right)_b}{N_b} \quad (3)$$

where N_a is the number of pixels in the band containing the RPE in one B-scan, I_{RPE_a} is the OCT signal in this band, N_b is the number of B-scans in each image collection, and N_{RPE} is the number of pixels (7 pixels or 33 μm) in the band containing the RPE in one B-scan.

Since the RTVue OCT does not record clustered data, we define $NRI(r,\theta)$ for one A-scan at radius *r* and azimuth angle θ as:

$$NRI(r,\theta)=\frac{\sum_{i=1}^{N_i} I_{RNFL_i}}{\overline{I}_{RPE}} \quad (4)$$

Where N_i is number of pixels in the RNFL in one A-scan, I_{RNFL_i} is the image intensity value in the RNFL and

$$\overline{I}_{RPE}=\frac{\sum_{b=1}^{N_b}\left(\sum_{a=1}^{N_a} I_{RPE_a}/N_{RPE}\right)_b}{N_b} \quad (5)$$

is the average OCT image intensity in the RPE averaged over all B-scans in one image collection, where N_a is the number of pixels in the band containing the RPE in one B-scan, I_{RPE_a} is the image intensity in this band, N_b is the number of B-scans in each image collection, and N_{RPE} is the number of pixels (7 pixels or 70 μm) in the band containing the RPE. For one imaging session, we calculate *NRI* for A-scans in one retinal scan and then construct an *NRI* map for that scan.

For both EIA and DEC OCT systems, seven RNFL locations were analyzed: all-rings, inner 5 rings, outer 5 rings, temporal (T), superior (S), nasal (N), and inferior (I) quadrants (Figure 1). For the RTVue OCT system, seven RNFL locations were analyzed: all-rings, inner 7 rings, outer 6 rings, temporal (T), superior (S), nasal (N), and inferior (I) quadrants.

The equations used to calculate RNFLT and NRI in the seven RNFL locations are given in Table 4.

Statistical analysis

The area under the Receiver Operating Characteristic (ROC) curve (AUC) was used to compare the performance of RNFLT and NRI for distinguishing between glaucoma and control subjects as well as between glaucoma-suspect and control subjects. Differences between areas under ROC curves were compared using a non-parametric method based on bootstrap sampling (n=2000 resamples). We used the pROC package[13] in the R statistical programming language (v2.15.10; http://www.R-project.org/, R Development Core Team, 2012, R Foundation for Statistical Computing, Vienna, Austria) and R studio (v0.94, RStudio, Inc.) for the ROC analysis. PASS 11 software (NCSS, Kaysville, Utah 84037) was used for statistical power and sample size calculations. Two sample t-test with equal variance was used for comparisons of the means of NRI and RNFLT of the glaucomatous, glaucoma-suspect, and control groups.

Results

We calculated the average NRI and RNFLT in seven RNFL locations. Pairwise comparisons among average NRI and RNFLT in different RNFL locations for distinguishing between glaucomatous and control eyes as well as between glaucoma-suspect and control eyes were made in terms of the area under the ROC curve. The average and standard deviation of NRI and RNFLT measured by PS-OCT-EIA, PS-OCT-DEC, and RTVue OCT in 7 RNFL locations of glaucomatous, glaucoma-suspect and control groups are shown in Table 5 and Table 6. For all three OCT instruments, NRIs of the control group are significantly larger than those of the glaucomatous group in all RNFL locations (p value shown in Table 6). NRIs of the control group are significantly larger than those of the glaucoma-suspect group in most RNFL locations (p value in Table 6).

Glaucomatous vs. control eyes

We identified the RNFL location that provided the largest AUC for each RNFL property for all three OCT instruments (values superscripted with "*" in Table 7,8 and 9; ROC curves shown in Figure 2). For the PS-OCT-EIA dataset, the all-rings average of *NRI* (NRI_{ALL}) and the inner-rings average of *RNFLT* ($RNFLT_{INNER}$) gave the largest AUCs. For PS-OCT-EIA data, a significant difference between *AUC* of $RNFLT_{INNER}$ and NRI_{ALL} was not observed (p=0.379) for the task of distinguishing between glaucomatous and control eyes.

The results for data collected by the PS-OCT-DEC system are similar to that collected by the PS-OCT-EIA system (Table 8). The *AUCs* of $RNFLT_{OUTER}$ and NRI_{OUTER} were not statistically significantly different (p=0.338) at distinguishing between glaucomatous and control eyes.

The RTVue OCT dataset was analyzed to investigate if the parameters for glaucoma diagnosis might vary for different OCT systems. For distinguishing control and glaucomatous eyes, the all-rings average of NRI (NRI_{ALL}) and $RNFLT_{ALL}$ provided the largest AUCs among all RNFL locations of NRI and RNFLT (superscripted with "*" in Table 9). A statistically significant difference between the AUC of NRI_{ALL} and that of $RNFLT_{ALL}$ for distinguishing glaucomatous and control eyes (p=0.877) was not observed. For the RTVue dataset, NRI_{ALL} and $RNFLT_{ALL}$ had similar performance for the task of distinguishing glaucomatous vs. control eyes. Thus, the results derived from the RTVue OCT dataset were consistent with those obtained from the other OCT datasets.

Glaucoma-suspect vs. control eyes

We also selected the RNFL location that provided the largest AUC value for each RNFL property (values superscripted with "*" in Table 10,11 and 12, ROC curves in Figure 3). For

distinguishing glaucoma-suspect vs. control eyes, NRI_{INNER} and $RNFLT_S$ exhibited the largest AUCs for the PS-OCT-EIA dataset. The comparisons between full AUCs of NRI_{INNER} and $RNFLT_S$ did not show any statistically significant difference (p=0.101).

For the PS-OCT-DEC dataset, NRI_{ALL} and $RNFLT_I$ had the largest AUCs for distinguishing glaucoma-suspect vs. control eyes The AUCs of NRI_{ALL} and $RNFLT_I$ did not show any statistically significant difference (p=0.227).

For RTVue OCT dataset, the inferior RNFL location gave the largest AUC for both NRI (NRI_I) and RNFLT ($RNFLT_I$) for distinguishing glaucoma-suspect from control eyes. The AUC of NRI_I was significantly larger than that of $RNFLT_I$ (p=0.008). Thus, NRI_I performs significantly better than $RNFLT_I$ at distinguishing glaucoma-suspect vs. control eyes.

DISCUSSION

In this human clinical study, a new OCT measured RNFL parameter, NRI, is introduced for glaucoma diagnosis. The diagnostic potential of NRI and RNFLT measured in seven RNFL locations (all-rings, inner-rings, outer-rings, and TSNI quadrants) is assessed to distinguish glaucomatous vs. control eyes as well as glaucoma-suspect vs. control eyes using data recorded by two custom-built PS-OCT systems and a commercial OCT system.

Since NRI can be computed similarly for all three OCT systems used in this study, measurement of NRI does not require introduction of new instrumentation or hardware modifications of existing systems. Computation of NRI requires only a software addition. Regardless of which OCT system was used to record retinal data, AUCs of NRI were always larger than those of RNFLT for distinguishing glaucoma-suspect vs. control eyes. The larger AUCs for NRI compared with RNFLT may be because both RNFL reflectance (RI) and RNFLT decrease with glaucoma. NRI is a unitless hybrid parameter that may also be less sensitive to RNFL boundary detection errors than either reflectance or RNFLT alone. RI as calculated in the primate study[9] does not improve glaucoma detection in this clinical study (see supplemental eTable 4–7). Results of this pilot clinical study suggest the need for a larger clinical study to validate the diagnostic power of NRI for identifying glaucoma at the pre-perimetric stage.

The average age of control subjects is significantly less than that of both the glaucoma and glaucoma-suspect groups as tested by two-sample t-test for two independent samples with equal variance in datasets from the Eye Institute of Austin (EIA) and Duke Eye Center (DEC) (Table 1). Therefore, RNFLT and NRI measurements might be biased by age difference in different groups since RNFLT decreases as age increases[14–17]. The relationship between NRI and age is unknown. However, the Pearson's correlation coefficient was evaluated between NRI measured by both custom OCT and RTVue OCT and age in the control, glaucoma, and glaucoma-suspect groups, respectively, and no statistically significant correlations were observed (p>0.5 for all groups as shown in supplemental eTable 2). From eTable 3, we observe no statistically significant correlations between RNFLT, measured by either of the PS-OCT instruments or RTVue OCT, and patient age in control, glaucoma, and glaucoma-suspect groups in our study. However, the finding that neither NRI nor RNFLT is statistically significant correlated with age may be due to the small sample size in our study. For example, for the control group in DEC, with the current sample size of 20 patients (which is the largest in our study) we achieve only an 11% power to detect a difference between a correlation of 0 and the observed correlation of −0.167 with a significance level of 0.05.

NRI as defined here is different than an RNFL reflectance parameter introduced in a previous study involving non-human primates.[9] Because NRI includes both RNFLT and reflectance, NRI can be considered as a combination feature of RNFLT and reflectance. Candidate cellular mechanisms that motivate why RNFL reflectance can be used as an early indicator of glaucoma were discussed previously.[9] The observed decrease in RNFL reflectance might be due to reduced collected backscatter due to intensified mitochondrial fission in early glaucoma resulting in increased large-angle scattering.[9]

In conclusion, a new parameter, NRI is introduced that may outperform RNFLT for distinguishing between glaucoma-suspect and control eyes. Results of this pilot clinical study suggest that NRI derived from OCT retinal images is a promising measure to detect pre-perimetric glaucoma.

Supplementary Material

Refer to Web version on PubMed Central for supplementary material.

Acknowledgments

Supported by National Eye Institute at the National Institutes of Health (Grant R01EY016462) and Research to Prevent Blindness (S.J.M.). Involved in design and conduct of the study (S.L., B.W., B.Y., T.E.M., M.K.M., S.J.M., H.G.R.); collection, management, analysis, and interpretation of the data (S.L., B.W., B.Y., T.E.M., M.K.M., S.J.M., H.G.R.); and preparation, review, or approval of the manuscript (S.L., B.W., B.Y., T.E.M., M.K.M., S.J.M., H.G.R.). The authors would like to thank Andrew W. Ross, M.D. for coordinating the study at EIA and Sara Crowell, M.S., CCRP for coordinating the study at DEC. The authors also thank Amit S. Paranjape, Ph.D. for his contribution to data collection at EIA and Andrew Klotz for his contribution to image processing of DEC data.

REFERENCES

1. Chang RT, Knight OJ, Feuer WJ, Budenz DL. Sensitivity and specificity of time-domain versus spectral-domain optical coherence tomography in diagnosing early to moderate glaucoma. Ophthalmology. Dec; 2009 116(12):2294–2299. [PubMed: 19800694]
2. Wu H, de Boer JF, Chen TC. Diagnostic capability of spectral-domain optical coherence tomography for glaucoma. Am J Ophthalmol. May; 2012 153(5):815–826. e812. [PubMed: 22265147]
3. Elmaanaoui B, Wang B, Dwelle JC, et al. Birefringence measurement of the retinal nerve fiber layer by swept source polarization sensitive optical coherence tomography. Opt Express. May 23; 2011 19(11):10252–10268. [PubMed: 21643283]
4. Hoh ST, Greenfield DS, Mistlberger A, Liebmann JM, Ishikawa H, Ritch R. Optical coherence tomography and scanning laser polarimetry in normal, ocular hypertensive, and glaucomatous eyes. Am J Ophthalmol. Feb; 2000 129(2):129–135. [PubMed: 10682963]
5. Sugimoto M, Ito K, Goto R, Uji Y. Symmetry analysis for detecting early glaucomatous changes in ocular hypertension using optical coherence tomography. Jpn J Ophthalmol. May-Jun;2004 48(3): 281–286. [PubMed: 15175923]
6. Anton A, Moreno-Montanes J, Blazquez F, Alvarez A, Martin B, Molina B. Usefulness of optical coherence tomography parameters of the optic disc and the retinal nerve fiber layer to differentiate glaucomatous, ocular hypertensive, and normal eyes. J Glaucoma. Jan; 2007 16(1):1–8. [PubMed: 17224742]
7. Caprioli J, Nouri-Mahdavi K, Law SK, Badala F. Optic disc imaging in perimetrically normal eyes of glaucoma patients with unilateral field loss. Trans Am Ophthalmol Soc. 2006; 104:202–211. [PubMed: 17471341]
8. Choi MG, Han M, Kim YI, Lee JH. Comparison of glaucomatous parameters in normal, ocular hypertensive and glaucomatous eyes using optical coherence tomography 3000. Korean J Ophthalmol. Mar; 2005 19(1):40–46. [PubMed: 15929486]

9. Dwelle J, Liu S, Wang B, et al. Thickness, phase retardation, birefringence, and reflectance of the retinal nerve fiber layer in normal and glaucomatous non-human primates. Invest Ophthalmol Vis Sci. Aug; 2012 53(8):4380–4395. [PubMed: 22570345]
10. Vermeer KA, van der Schoot J, Lemij HG, de Boer JF. RPE-normalized RNFL attenuation coefficient maps derived from volumetric OCT imaging for glaucoma assessment. Invest Ophthalmol Vis Sci. Aug 14.2012
11. Wang B, Paranjape A, Yin B, et al. Optimized Retinal Nerve Fiber Layer Segmentation Based on Optical Reflectivity and Birefringence for Polarization-Sensitive Optical Coherence Tomography. Paper presented at: Proc. SPIE. 2011
12. Kass M, Witkin A, Terzopoulos D. Snakes: Active contour models. International Journal of Computer Vision. 1988; 1(4):321–331.
13. Robin X, Turck N, Hainard A, et al. pROC: an open-source package for R and S+ to analyze and compare ROC curves. BMC Bioinformatics. 2011; 12:77. [PubMed: 21414208]
14. Alamouti B, Funk J. Retinal thickness decreases with age: an OCT study. Br J Ophthalmol. Jul; 2003 87(7):899–901. [PubMed: 12812895]
15. Bowd C, Zangwill LM, Blumenthal EZ, et al. Imaging of the optic disc and retinal nerve fiber layer: the effects of age, optic disc area, refractive error, and gender. J Opt Soc Am A Opt Image Sci Vis. Jan; 2002 19(1):197–207. [PubMed: 11778725]
16. Varma R, Skaf M, Barron E. Retinal nerve fiber layer thickness in normal human eyes. Ophthalmology. Dec; 1996 103(12):2114–2119. [PubMed: 9003346]
17. Leung CK, Yu M, Weinreb RN, et al. Retinal nerve fiber layer imaging with spectral-domain optical coherence tomography: a prospective analysis of age-related loss. Ophthalmology. Apr; 2012 119(4):731–737. [PubMed: 22264886]

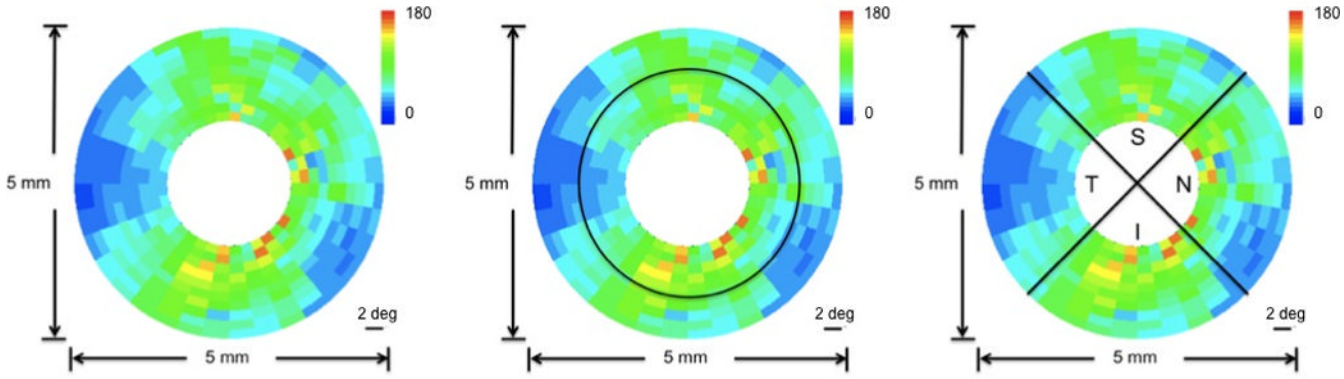

Figure 1.

Definitions of analyzed RNFL locations of EIA and DEC OCT datasets illustrated on a clustered RNFLT map of a human eye (OD). Average computed across all-rings (left panel). Averages computed over 5 inner rings (inner) and 5 outer rings (outer) (middle panel). Averages computed over the temporal (T), superior (S), nasal (N) and inferior (I) quadrants (right panel).

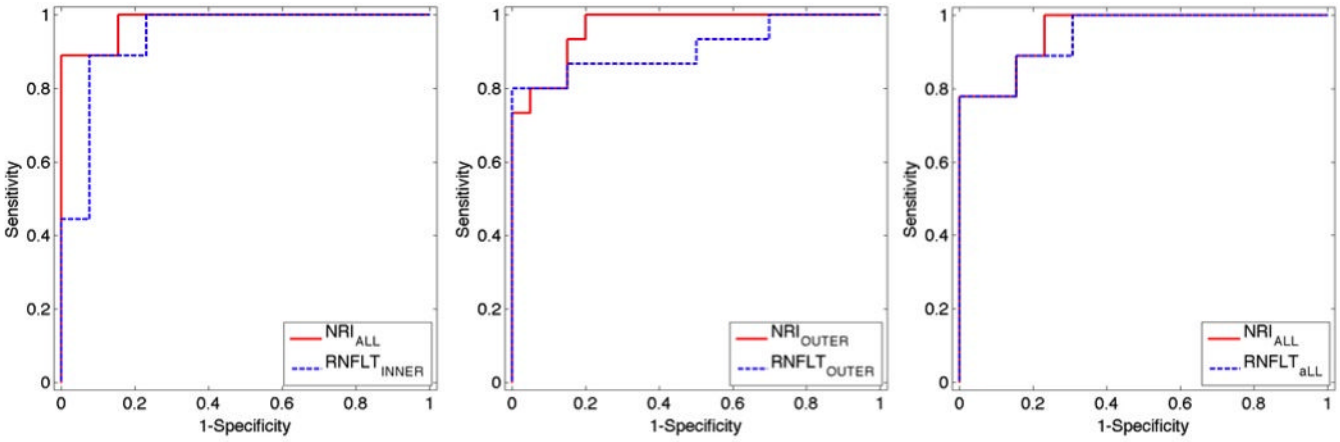

Figure 2.

ROCs of NRI_{ALL} and $RNFLT_{INNER}$ for distinguishing glaucomatous vs. control eyes for PS-OCT-EIA dataset (left). ROCs of NRI_{OUTER} and $RNFLT_{OUTER}$ for distinguishing glaucomatous vs. control eyes for PS-OCT-DEC dataset (middle). ROC curves of NRI_{ALL} and $RNFLT_{ALL}$ for distinguishing glaucomatous vs. control eyes for RTVue OCT dataset (right).

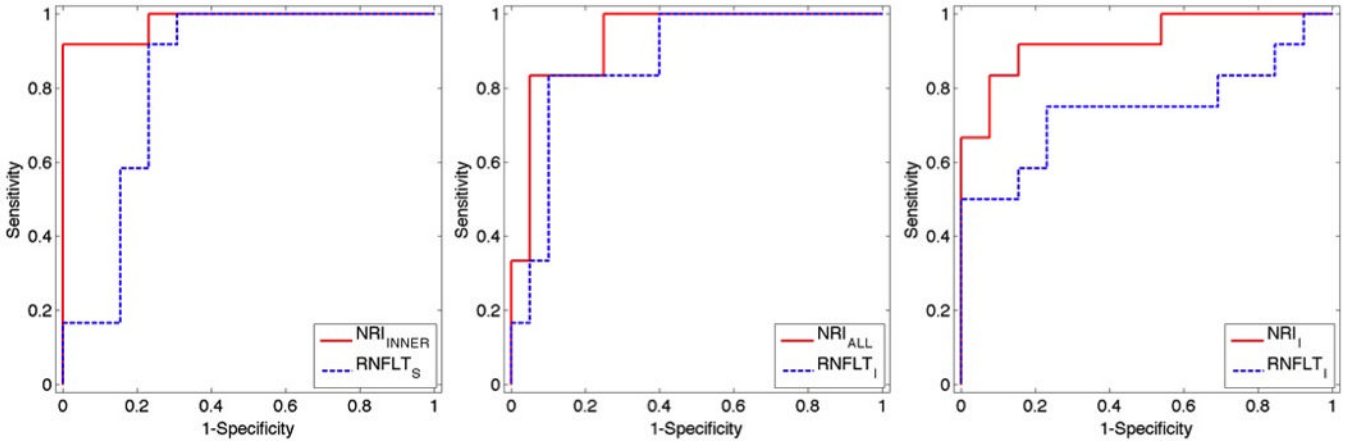

Figure 3.

ROCs of NRI_{INNER} and $RNFLT_S$ for distinguishing glaucoma-suspect vs. control eyes from PS-OCT-EIA data (left). ROCs of NRI_{ALL} and $RNFLT_I$ for distinguishing glaucoma-suspect vs. control eyes from PS-OCT-DEC data (middle). ROC curves of NRI_I and $RNFLT_I$ for distinguishing glaucoma-suspect vs. control eyes for the RTVue OCT dataset (right).

Table 1

Mean-age and standard deviation together with gender distribution, mean and standard deviation of visual field mean deviation (VF MD) and visual field pattern standard deviation (VF PSD) of control (ct), glaucomatous (gl), and glaucoma-suspect (gs) eyes imaged by PS-OCT-EIA, PS-OCT-DEC and RTVue OCT.

PS-OCT-EIA		ct (n=13)	gl (n=9)	gs (n=12)
	Age (years)	54.46 ± 7.60	65.56 ± 6.39	66.17 ± 8.30
	Gender			
	Male	3	4	6
	Female	10	5	6
	VF MD	-0.33 ± 1.49	-3.02 ± 2.13	-0.57 ± 1.65
	VF PSD	1.98 ± 1.07	4.83 ± 3.17	2.24 ± 1.93
PS-OCT-DEC		ct (n=20)	gl (n=15)	gs (n=6)
	Age (years)	58.25 ± 7.47	67.27 ± 6.40	66.00 ± 8.15
	Gender			
	Male	9	4	2
	Female	11	11	4
	VF MD	-0.54 ± 1.86	-5.00 ± 4.82	0.58 ± 1.99
	VF PSD	2.17 ± 1.45	6.14 ± 4.46	1.80 ± 0.29
RTVue OCT		ct (n=13)	gl (n=9)	gs (n=12)
	Age (years)	54.46 ± 7.60	65.56 ± 6.39	66.17 ± 8.30
	Gender			
	Male	3	4	6
	Female	10	5	6
	VF MD	0.10 ± 1.20	-3.00 ± 2.15	-0.35 ± 1.58
	VF PSD	1.98 ± 1.10	4.42 ± 3.39	1.73 ± 0.53

Table 2

Inclusion and exclusion criteria for the study.

Inclusion criteria		Exclusion criteria	
1	age between 40 and 80 years;	**1**	discernable anomaly of the anterior chamber;
2	visual acuity score of 20/40 or better;	**2**	uveitis;
3	spherical refractive error within ± 5 diopters;	**3**	significant opacification of the cornea or crystalline lens;
4	cylinder refractive error within ± 3 diopters.	**4**	concurrent active eye disease in the study eye that may affect intraocular pressure (IOP) or its measurement;
		5	secondary glaucoma or acute narrow-angle glaucoma;
		6	pigmentary or pseudoexfoliation glaucoma;
		7	proliferative or severe nonproliferative diabetic retinopathy, retinal detachment retinitis pigmentosa, or other significant retinopathy;
		8	visual field loss attributed to a non-glaucoma condition;
		9	dilated pupil diameter less than 4mm, and visual field constriction less than 20 degrees;
		10	patients undergoing kidney dialysis;
		11	any physical or mental impairment adversely affecting study participation.

Table 3

Definitions of control, glaucoma, and glaucoma-suspect.

Control	Glaucoma	Glaucoma-suspect*
Has an intraocular pressure (IOP) less than 21 mmHg with no history of elevated IOP, normal visual fields [mean deviation and pattern standard deviation (PSD) within 95% confidence limits and Glaucoma Hemifield Test (GHT) within normal limits], and no optic disc abnormalities judged by a glaucoma specialist (H.G.R. at EIA and S.J.M. at DEC).	Has history of elevated IOP, two consecutive abnormal visual fields (PSD outside the 95% confidence limits, abnormal GHT, or any typical visual field defect), and an abnormal optic disc.	Ocular hypertension: Has an IOP higher than 21 mmHg but less than 30 mmHg measured in at least three separate office visits and have normal optic nerve head appearance. Preperimetric glaucoma: Has an asymmetric cup-to-disc ratio and show early glaucomatous optic disc abnormality, including thinning of the neuroretinal rim and notching.

*All subjects belonging to the glaucoma-suspect group have normal visual field test results as defined in the control group.

Table 4

The calculation of average values of *RNFLT(r,θ)* and *NRI(r,θ)* in seven RNFL locations.

RNFL location	Equation	Instrument-specific RNFL properties
All rings	$P_{ALL}=\frac{\sum_{r=r_{in}}^{r_{out}}\sum_{\theta=0^\circ}^{360^\circ}P(r,\theta)}{N_a}$	$P(r\theta)$ – RNFL properties including RNFLT($r\theta$) or NRI($r\theta$). r_{in} – the radius of the innermost scanning ring. r_{out} – the radius of the outermost scanning ring. N_a – total number of A-scans in one measurement. N_{INNER} – number of A-scans in inner rings. N_{OUTER} – number of A-scans in outer rings. N_S – number of A-scans in superior quadrant. N_I – number of A-scans in inferior quadrant. N_N – number of A-scans in nasal quadrant. N_T – number of A-scans in temporal quadrant. **PS-OCT-EIA:** r_{in} = 1 mm r_{out} = 2.5 mm N_a = 36000 (100 A-scan/cluster × 36 clusters/ring × 10 rings) **PS-OCT-DEC:** r_{in} = 0.75 mm r_{out} = 2.5 mm N_a = 36000 (100 A-scan/cluster × 36 clusters/ring × 10 rings) **RTVue OCT:** r_{in} = 0.65 mm r_{out} = 2.45 mm N_a = 8681 (425 A-scan/ring × 4 rings + 587 A-scan/ring × 3 rings + 775 A-scan/ring × 3 rings + 965 A-scan/ring × 3 rings)
Inner rings	$P_{INNER}=\frac{\sum_{r=r_{in}}^{(r_{out}+r_{in})/2}\sum_{\theta=0^\circ}^{360^\circ}P(r,\theta)}{N_{INNER}}$	
Outer rings	$P_{OUTER}=\frac{\sum_{r=(r_{out}+r_{in})/2}^{r_{out}}\sum_{\theta=0^\circ}^{360^\circ}P(r,\theta)}{N_{OUTER}}$	
Superior	$P_S=\frac{\sum_{r=r_{in}}^{r_{out}}\sum_{\theta=45^\circ}^{135^\circ}P(r,\theta)}{N_S}$	
Inferior	$P_I=\frac{\sum_{r=r_{in}}^{r_{out}}\sum_{\theta=225^\circ}^{315^\circ}P(r,\theta)}{N_I}$	
Nasal	OS: $P_N=\frac{\sum_{r=r_{in}}^{r_{out}}\sum_{\theta=135^\circ}^{225^\circ}P(r,\theta)}{N_N}$	
	OD: $P_N=\frac{\sum_{r=r_{in}}^{r_{out}}\left(\sum_{\theta=315^\circ}^{360^\circ}P(r,\theta)+\sum_{\theta=0^\circ}^{45^\circ}P(r,\theta)\right)}{N_N}$	
Temporal	OS: $P_T=\frac{\sum_{r=r_{in}}^{r_{out}}\left(\sum_{\theta=315^\circ}^{360^\circ}P(r,\theta)+\sum_{\theta=0^\circ}^{45^\circ}P(r,\theta)\right)}{N_T}$	
	OD: $P_T=\frac{\sum_{r=r_{in}}^{r_{out}}\sum_{\theta=135^\circ}^{225^\circ}P(r,\theta)}{N_T}$	

Table 5

The average and standard deviation of RNFLT measured by PS-OCT-EIA, PS-OCT-DEC and RTVue OCT in 7 RNFL locations of glaucomatous (gl), glaucoma-suspect (gs) and control (ct) groups.

	RNFLT (μm)	**ct (n=13)**	**gl (n=9)**	**gs (n=12)**	**p value of gl vs. ct**	**p value of gs vs. ct**
PS-OCT-EIA	ALL rings	84.058 ± 13.539	65.652 ± 2.962	70.387 ± 11.168	0.00036*	0.00583*
	INNER rings	93.343 ± 14.182	73.150 ± 4.469	77.586 ± 11.740	0.00028*	0.00311*
	OUTER rings	72.9 27 ±12.748	57.672 ± 3.174	63.226 ± 11.466	0.00115*	0.02907*
	Superior	99.292 ± 17.518	77.462 ± 8.426	75.939 ± 11.742	0.00126*	0.00038*
	Inferior	94.074 ± 16.764	70.147 ± 14.651	77.062 ± 13.814	0.00124*	0.00563*
	Nasal	75.399 ± 20.390	64.803 ± 10.015	65.919 ± 5.705	0.08324	0.06702
	Temporal	65.693 ± 13.826	49.648 ± 10.009	62.562 ± 32.709	0.00375*	0.37731
PS-OCT-DEC	**RNFLT (μm)**	**ct (n=20)**	**gl (n=15)**	**gs (n=6)**		
	ALL rings	67.511 ± 4.479	58.730 ± 5.410	62.484 ± 3.664	0.00000*	0.00984*
	INNER rings	70.736 ± 7.045	61.604 ± 6.965	65.314 ± 3.534	0.00029*	0.04226*
	OUTER rings	64.454 ± 4.780	55.651 ± 4.866	59.939 ± 5.556	0.00000*	0.03093*
	Superior	76.470 ± 12.235	63.502 ± 10.656	67.817 ± 7.511	0.00124*	0.05821
	Inferior	73.212 ± 9.293	61.957 ± 7.774	60.951 ± 8.425	0.00030*	0.00404*
	Nasal	62.939 ± 12.728	57.342 ± 6.319	62.791 ± 8.115	0.06406	0.48946
	Temporal	57.215 ± 9.665	52.179 ± 6.498	57.775 ± 9.485	0.04547*	0.54918
RTVue OCT	**RNFLT (μm)**	**ct (n=13)**	**gl (n=9)**	**gs (n=12)**		
	ALL rings	125.293 ± 12.514	98.673 ± 12.624	114.804 ± 17.194	0.00004*	0.04635*
	INNER rings	153.603 ± 19.016	117.046 ± 16.828	140.348 ± 24.304	0.00008*	0.07039*
	OUTER rings	92.264 ± 6.793	77.234 ± 8.474	85.003 ± 9.349	0.00008*	0.01772*
	Superior	157.290 ± 18.123	124.313 ± 18.901	139.969 ± 22.671	0.00026*	0.02258*
	Inferior	160.741 ± 13.343	122.047 ± 22.750	144.199 ± 20.848	0.00003*	0.01292*
	Nasal	94.652 ± 18.365	69.255 ± 9.165	87.178 ± 22.398	0.00054*	0.18470
	Temporal	88.487 ± 12.132	79.074 ± 16.933	87.864 ± 14.667	0.07164	0.45429

Table 6

The average and standard deviation of NRI measured by PS-OCT-EIA, PS-OCT-DEC and RTVue OCT in 7 RNFL locations of glaucomatous (gl), glaucoma-suspect (gs) and control (ct) groups.

	NRI	ct (n=13)	gl (n=9)	gs (n=12)	p value of gl vs. ct	p value of gs vs. ct
PS-OCT-EIA	ALL rings	2226.369 ± 219.516	1633.200 ± 224.668	1720.683 ± 178.260	0.00000*	0.00000*
	INNER rings	2489.908 ± 257.980	1812.722 ± 312.250	1896.192 ± 224.131	0.00001*	0.00000*
	OUTER rings	1909.754 ± 174.941	1455.778 ± 242.103	1543.258 ± 155.460	0.00003*	0.00001*
	Superior	2549.269 ± 440.515	1867.433 ± 192.533	1845.283 ± 270.317	0.00016*	0.00004*
	Inferior	2540.662 ± 316.212	1786.278 ± 592.825	1903.775 ± 322.501	0.00046*	0.00002*
	Nasal	2049.346 ± 399.788	1525.800 ± 197.058	1626.658 ± 158.909	0.00086*	0.00118*
	Temporal	1720.054 ± 295.773	1297.898 ± 310.042	1486.797 ± 606.125	0.00211*	0.11402
PS-OCT-DEC	**NRI**	**ct (n=20)**	**gl (n=15)**	**gs (n=6)**		
	ALL rings	1562.440± 190.372	1100.141± 191.161	1221.933± 170.761	0.00000*	0.00032*
	INNER rings	1635.695± 259.396	1148.511± 228.728	1316.150± 201.610	0.00000*	0.00541*
	OUTER rings	1497.005± 198.606	1043.759± 169.603	1148.588± 223.010	0.00000*	0.00060*
	Superior	1801.783± 429.505	1217.025± 333.845	1368.400± 215.503	0.00006*	0.01339*
	Inferior	1710.158± 330.698	1114.308± 270.276	1198.192± 327.767	0.00000*	0.00139*
	Nasal	1407.556± 383.236	1057.143± 180.055	1213.545± 312.360	0.00125*	0.13529
	Temporal	1299.774± 301.778	979.251± 184.080	1090.285± 263.628	0.00047*	0.06960
RTVue OCT	**NRI**	**ct (n=13)**	**gl (n=9)**	**gs (n=12)**		
	ALL rings	13.001± 2.066	8.110± 2.166	9.957± 1.772	0.00002*	0.00033*
	INNER rings	15.230± 2.999	9.106± 2.402	11.411± 2.522	0.00003*	0.00114*
	OUTER rings	10.401± 1.343	6.948± 2.148	8.260± 1.143	0.00008*	0.00014*
	Superior	16.066± 2.889	9.777± 3.083	11.736± 2.965	0.00004*	0.00059*
	Inferior	17.149± 2.519	10.495± 3.313	12.585± 1.864	0.00002*	0.00002*
	Nasal	9.614± 2.385	5.890± 1.773	7.304± 2.069	0.00037*	0.00843*
	Temporal	9.174± 1.798	6.278± 1.841	8.202± 2.587	0.00074*	0.14166

J Glaucoma. Author manuscript; available in PMC 2015 January 01.

Table 7

AUC and its standard error of NRI and RNFLT averaged over seven RNFL locations for PS-OCT-EIA dataset for distinguishing glaucomatous vs. control eyes.

RNFL location	Glaucomatous vs. Control	
	NRI	*RNFLT*
	AUC	AUC
ALL rings	0.983 ± 0.021*	0.932 ± 0.056
INNER rings	0.923 ± 0.078	0.940 ± 0.050*
OUTER rings	0.966 ± 0.032	0.897 ± 0.071
Superior	0.923 ± 0.060	0.872 ± 0.076
Inferior	0.872 ± 0.086	0.889 ± 0.068
Nasal	0.872 ± 0.076	0.735 ± 0.112
Temporal	0.838 ± 0.096	0.838 ± 0.089

Table 8

AUC and its standard errors of *NRI and RNFLT* averaged over seven RNFL locations for the PS-OCT-DEC dataset for distinguishing glaucomatous vs. control eyes.

RNFL location	Glaucomatous vs. Control	
	NRI	***RNFLT***
	AUC	**AUC**
ALL rings	0.957 ± 0.032	0.880 ± 0.065
INNER rings	0.947 ± 0.037	0.790 ± 0.083
OUTER rings	0.963 ± 0.026*	0.910 ± 0.058*
Superior	0.860 ± 0.063	0.783 ± 0.081
Inferior	0.920 ± 0.044	0.837 ± 0.071
Nasal	0.813 ± 0.075	0.635 ± 0.097
Temporal	0.823 ± 0.073	0.657 ± 0.095

Table 9

AUC and standard errors for distinguishing glaucomatous vs. control eyes of NRI and RNFLT averaged over seven RNFL locations from the RTVue OCT dataset.

RNFL location	Glaucomatous vs. Control	
	NRI	RNFLT
	AUC	AUC
ALL rings	0.957 ± 0.037*	0.949 ± 0.043*
INNER rings	0.957 ± 0.037	0.940 ± 0.046
OUTER rings	0.949 ± 0.043	0.932 ± 0.054
Superior	0.949 ± 0.043	0.897 ± 0.065
Inferior	0.949 ± 0.043	0.906 ± 0.074
Nasal	0.923 ± 0.059	0.915 ± 0.061
Temporal	0.872 ± 0.075	0.726 ± 0.124

Table 10

AUC and standard errors for distinguishing glaucoma-suspect vs. control eyes of NRI and RNFLT from the PS-OCT-EIA dataset averaged over seven RNFL locations.

RNFL location	Control vs. Glaucoma-suspect	
	NRI	RNFLT
	AUC	AUC
ALL rings	0.968 ± 0.034	0.821 ± 0.094
INNER rings	0.981 ± 0.022*	0.808 ± 0.089
OUTER rings	0.955 ± 0.041	0.788 ± 0.101
Superior	0.897 ± 0.064	0.833 ± 0.092*
Inferior	0.936 ± 0.047	0.801 ± 0.089
Nasal	0.782 ± 0.101	0.756 ± 0.107
Temporal	0.769 ± 0.104	0.660 ± 0.117

Table 11

AUC and standard errors for distinguishing glaucoma-suspect vs. control eyes of NRI and RNFLT from the PS-OCT-DEC dataset averaged over seven RNFL locations.

RNFL location	Control vs. Glaucoma-suspect	
	NRI	RNFLT
	AUC	AUC
All rings	0.933 ± 0.052*	0.850 ± 0.077
Inner rings	0.833 ± 0.117	0.800 ± 0.110
Outer rings	0.908 ± 0.063	0.742 ± 0.130
Superior	0.808 ± 0.085	0.750 ± 0.134
Inferior	0.867 ± 0.088	0.875 ± 0.077*
Nasal	0.583 ± 0.145	0.483 ± 0.133
Temporal	0.667 ± 0.124	0.450 ± 0.142

Table 12

AUC and standard errors for distinguishing glaucoma-suspect vs. control eyes based on NRI and RNFLT averaged over seven RNFL locations from the RTVue OCT dataset.

RNFL location	Glaucoma-suspect vs. Control	
	NRI	RNFLT
	AUC	AUC
ALL rings	0.885 ± 0.066	0.679 ± 0.118
INNER rings	0.833 ± 0.081	0.673 ± 0.116
OUTER rings	0.878 ± 0.073	0.744 ± 0.106
Superior	0.846 ± 0.085	0.724 ± 0.106
Inferior	0.929 ± 0.052*	0.744 ± 0.110*
Nasal	0.763 ± 0.104	0.667 ± 0.118
Temporal	0.622 ± 0.125	0.487 ± 0.124